Published in final edited form as:
Opt Express. 2008 October 27; 16(22): 17903–17914.

Methodology development for three-dimensional MR-guided near infrared spectroscopy of breast tumors◇

Colin M. Carpenter, **Subhadra Srinivasan**, **Brian W. Pogue**, and **Keith D. Paulsen**
Thayer School of Engineering, Dartmouth College Hanover, N.H., 03755

Abstract

Combined Magnetic Resonance (MR) and Near Infrared Spectroscopy (NIRS) has been proposed as a unique method to quantify hemodynamics, water content, and cellular size and packing density of breast tumors, as these tissue constituents can be quantified with increased resolution and overlaid on the structural features identified by the MR. However, the choices in how to reconstruct and visualize this information can have a dramatic impact on the feasibility of implementing this modality in the clinic. This is especially true in 3 dimensions, as there is often limited optical sampling of the breast tissue, and methods need to accurately reflect the tissue composition. In this paper, the implementation and display of fully 3D MR image-guided NIRS is outlined and demonstrated using *in vivo* data from three healthy women and a volunteer undergoing neoadjuvant chemotherapy. Additionally, a display feature presented here scales the transparency of the optical images to the sensitivity of the measurements, providing a logical way to incorporate partial volume sets of optical images onto the MR volume. These concepts are demonstrated with 3D data sets using Volview software online.

1. Introduction

The current standard of care in breast cancer imaging, consisting of ultrasound, xray, and MR mammography, only provides a fraction of the total available information that could be obtained diagnostically. It is not surprising then, that there has been considerable effort in identifying new approaches which attempt to improve upon the unsatisfactory specificity [1, 2,3] of breast cancer imaging. The ideal approach would add additional contrast to these systems to discriminate malignant tumors from the surrounding benign or healthy tissue [4,5, 6,7,8]. The integration of optics into standard breast cancer imaging systems is one promising area. Optical imaging provides functional information which should improve lesion characterization, thereby reducing unnecessary breast biopsies. Innovations to improve its capabilities have included better instrumentation, more sophisticated computational algorithms, contrast agents, and more recently, image guided approaches which integrate the higher resolution of a complimentary modality into optical imaging to improve contrast recovery [9,10]. While several pilot studies using this method have been carried out [9,11], a major factor limiting more comprehensive studies has been the lack of a practical approach to combine these modalities. This paper discusses the latest software tools and methodology which have enabled three-dimensional MR-guided diffuse optical imaging of breast cancer *in vivo* to become a practical procedure.

◇Datasets associated with this article are available at http://hdl.handle.net/ 10376/1063.

E-mail: colinc@dartmouth.edu.

A synergistic multimodal approach is possible when one modality provides good structural feature identification, while the other provides functional or molecular information about the features [12]. MR imaging has encouraged perhaps more multimodality interest than xray mammography recently because its extremely high sensitivity might enable a complimentary technology to aid in specificity. Diffuse optical tomography (DOT) can fill this need because it gives information about tissue health by providing images of total hemoglobin, hemoglobin oxygen saturation, water content, lipid content, and scattering properties. Breast cancers have been shown in select studies to have higher hemoglobin and water content than normal tissue, and lower lipid content [13,14,15,16,17]. This technique has shown varying degrees of success, depending on study protocol [18,19], and generally improves upon the specificity of breast characterization. However, the accuracy of optical mammography with small lesions below the resolution limit of $\sim\frac{1}{2}$ cm is limited, as both larger-scale studies either noted poorer characterization of lesions (< 6mm) [19], or excluded them altogether [18]. It has been shown that the inclusion of high resolution spatial guidance from xray or MR improves the spatial resolution and quantification of optical imaging [20,21,22], often by as much as 35%, depending on technique [23].

To date, most clinical studies of optical mammography involving the use of multimodality spatial guidance have been focused on planar acquisitions limited to two dimensions for practical reasons. Yet optical imaging in three dimensions is critical because of the more accurate models of light propagation in 3D, and the difficulty in positioning the optical probes directly over the region of interest with planar or sparse data sampling, especially when the lesion is not palpable. Additionally, there is a need to modify 3D visualization tools to appropriately weight the display of optical data to the sensitivity of the measurements, so that clinicians are not mislead about reconstructed tissue contents which may lie far outside the sampling volume.

The main reason for this limitation in technique has to date been the computational burden of volumetric reconstruction, as shown in Figure 1, and the effects of poorly sampled tissues on the inverse problem. It is clear that when advancing DOT or simultaneous MR-DOT to three dimensions, the number of unknowns grows by orders of magnitude. However, by using the MR to guide the separation of unique tissue types which can be characterized spectroscopically (MRg-NIRS), this modality becomes much more practical, and yet preserves the spatial fidelity of the original MR images. This paper presents the methodology and implementation of reconstruction and visualization of MR-guided NIRS in three dimensions, and results from phantom experiments and female breast tissue *in vivo*.

2. Methods

2.1. Instrumentation

The MR-NIRS system uses 6 intensity modulated laser diodes in the near infrared spectrum to illuminate the breast tissue. Sixteen fiber bundles are bifurcated so that the source and detector fibers are housed in the same optodes which are in contact with the skin. Source positions are moved sequentially around the breast while the amplitude and phase of transmitted light is detected with photomultiplier tubes at 15 detector locations for each source position. Fiber bundles pass through a conduit from the MR console room into the MR scanner room and into a patient interface which clips on to a commercial breast MR coil. More details about the instrumentation can be found in [10].

This study used a 3 Tesla Philips Achieva magnet to acquire anatomical and contrast enhanced images used in the optical image reconstruction procedure [24]. Specifically, T1-weighted Spin Echo (TR/TE = 900/10, flip angle = 90°) MR images are taken to differentiate between adipose

and fibroglandular tissue. Dynamic Contrast Enhanced MR (DCE-MR) is acquired by injecting an MR contrast agent (Magnavist, Schering) intravenously, and taking sets of T1-W Gradient Echo volume images (TR/TE = 10/6, flip angle 20°) each minute. Contrast subtraction images are formed by subtracting the post contrast dynamic images from the pre contrast images. These images are used to identify suspect lesions, which are also confirmed as suspicious by a radiologist (S.P., R.D-A).

Coregistration between the optical and MRI domains requires knowledge of the location of the optical fibers in the MR anatomical images. Because the optical and MRI data are taken simultaneously, these modalities can be accurately coregistered to within 1mm. The optical fibers can be located in the MR image by identifying the displacement of the tissue caused by the contact between the tissue and the fibers, which extend beyond the breast immobilization plate by 1mm. MR radiological fiducial markers are also used to identify various points of reference in the MR domain.

2.2. Image Formation

A model based image reconstruction algorithm has been used which minimizes the mismatch between the amplitude and phase data collected from the system and a diffusion based model for three-dimensional light propagation in tissue [25,26]. The lossy diffusion equation, which describes light fluence (**Φ**) in tissue from source S with frequency (ω), has been well studied in turbid media such as tissue, and is an acceptable approximation if scattering (μ_s') dominates over absorption (μ_a), and if source detector distances are more than a few scattering distances apart [27].

$$-\nabla \cdot D\nabla\Phi(r,\omega) + \left(\mu_a + \frac{i\omega}{c}\right)\Phi(r,\omega) = S(r,\omega) \tag{1}$$

Here, D is the diffusion coefficient, defined as $\frac{1}{(3(\mu_s' + \mu_a))}$. Since parameter estimation problems are non-linear, the image formation algorithm, shown below in Eq. (2), uses an iterative procedure based on a Newton-type minimization method [28] to find the best estimate for the physiological parameters c: oxy hemoglobin, deoxy hemoglobin, water, scatter power, and scatter amplitude [29,30]. Here, J is the Jacobian matrix, I is the Identity matrix, and δ is the difference between the collected data and the model data produced by Eq. (1).

$$\left(J^T J + \lambda I\right)\Delta c = J^T \Delta\delta \tag{2}$$

This equation is known to be ill-posed and is often underdetermined. This is especially true in 3D, and many strategies have been introduced to alleviate the associated effects by constraining the allowed solution space. We use an iterative Tikhanov optimization routine which adds a regularization parameter, λ , to eliminate improbable solutions [31]. This parameter requires information on both the noise of the system and limitations on the contrast of the imaging domain, and is highly influential on the solutions [32]. This term can be problematic and may seem somewhat arbitrary, as coupling errors which introduce noise are difficult to quantify [33], and determining limitations on contrast is a problem which is case and situation specific.

The incorporation of MR information into the reconstruction algorithm helps solve the dependence of the solution on this parameter, because it alleviates the ill-posed nature of the problem by reducing the parameter space to a set number of tissue types and regions of interest (ROIs). This reduces the unknown parameter space considerably. Additionally, because the

high structural resolution is kept intact, this spectroscopic approach is advantageous over other image guided techniques which use the tissue regions only to infer information about tissue contrast [22,21]. This technique also reduces the burden of reconstructing for features which are so far from the imaging plane that they have no contribution to the data. Reduction in parameters is done by summing the contributions from unknowns in each region in the jacobian; the technique is explained in more detail in a previous publication [25]. Using this technique, solutions are less affected by noise. In this study, image reconstructions were calculated with a regularization parameter of 10. However, recovered values were quite immune to changes in the regularization parameter. With the addition of the high resolution structural information provided by the MR, the imaging procedure becomes a volumetric spectroscopy problem.

2.3. From MR Images to Computational Domains

Incorporating MR images into the image reconstruction is non-trivial in 3D, and much effort has gone into processing these irregular shaped domains. The steps from image segmentation to volumetric meshing and region labeling are overviewed in Figure 2. Tissue types were identified in 3D with a commercial software package (Mimics, Materialise NV). Structural MR (T1-W) images were taken to separate the adipose tissue from the fibroglandular tissue. Dynamic contrast enhanced MR was used to delineate suspect regions of interest from the background. These MR images were all taken in the same geometry, so volumes segmented from the DCEMR could be imported directly into the structural MR image. The outer surface of the adipose layer was input into a software package MIVA [34] to create a volumetric finite element mesh required to solve Eq. (1). This mesh was imported back into Mimics and tagged with tissue material region labels for use in the image reconstruction algorithm. The meshes used in this study had an average of 2.5 mm/node resolution, which usually formed meshes of 40,000 nodes.

2.4. 3-Dimensional Image Visualization

The images presented in this paper show recovered contrast in each MR-defined tissue type. However, images presented in this way can be misleading because of the decrease in sensitivity of the detectors to contrasts at distance. The distance limit on contrast recovery depends on both the intrinsic contrast and the system properties. Therefore, the volumes presented in this work have used a transparency setting which is proportional to the sensitivity of the measurements to the contrast in each tissue voxel. This relation, the Jacobian, is shown in Eq. (3), where β is a scaling parameter which is adjusted so that the transparency is zero 1 cm above the center fiber array, and $\mathbf{\Phi}$ is the amplitude for absorbing and phase for scattering chromophores, c. By scaling the transparency to the Jacobian matrix values, tissue properties far outside the imaging plane will not be seen and misinterpreted as true contrasts.

$$\alpha=\beta\frac{\partial\Phi}{\partial c} \tag{3}$$

2.5. Human Subject Imaging

Imaging protocol for the subject examinations was approved by the Committee for the Protection of Human Subjects at Dartmouth Hitchcock Medical Center. Written consent was obtained from all subjects. The subjects were positioned in the MR breast coil on the MR table and optical fibers in a slab type geometry were brought into contact with the tissue. Because of the desire for light compression, some optical fibers on some exams did not contact the breast, but at least 14 of 16 were in contact for all exams. Optical fibers were located on MR images taken in the sagittal or axial geometries with the aid of fiducial markers placed on the

optical interface. Optical exams were performed simultaneously with MR exams, and usually took about 15 minutes. MR exams were completed within 45 minutes.

3. Results

3.1. Phantom Imaging Results

The accuracy of MR guided NIRS in 3D was tested on a gelatin phantom with a cylindrical inclusion 1.6 cm in diameter in a slab (12 × 6.4 cm). For the background, porcine blood was mixed at the appropriate concentration into a solution of Phosphate Buffered Saline (PBS), gelatin, and titanium oxide particles once the temperature of the stirring mixture cooled sufficiently. This solution was cooled in a refrigerator with a test tube sunk near the boundary until the solution set into a hard phantom. A mixture of PBS, intralipid, and porcine blood was added to the hole remaining from the extracted test tube. The inclusion had an expected value for total hemoglobin of 0.02 milliMolar (mM), and the background of 0.01 mM, for an expected contrast of 2:1. There was no contrast expected in water, which was quantified using MRI 3-Point Dixon water fat separation. There was no expected contrast in scatter, as the appropriate amount of intralipid was added to match the scattering of the background, as confirmed by imaging of the bulk solution in the system. Figure 3(a) shows a T2-W MR image of the phantom. The reconstructed results shown in Figure 3(b) show that total hemoglobin in the inclusion reaches the expected value. The background total hemoglobin is elevated by about 60% over the expected contrast. This could be explained from the crosstalk between water and oxy-hemoglobin which is expected because of the limitation of the PMT optical detectors in the long wavelengths above 850nm as discussed below. However, this crosstalk is expected to be greater in this phantom than in human tissue because gelatin mixtures have nearly twice the water of human tissue. The variations in oxygen saturation and water were just over 6%, and the variations for scatter amplitude and power were just over 8% and 37%.

3.2. Human Breast Imaging Results

3D imaging of breast tissue was applied to data from three healthy subjects. The patient interface was adjusted to apply light compression to the breast so that the optodes were in contact with the breast. Figure 4 shows the results which are comparable to previously published 2D results of 11 subjects with the same system [11], and are in the range typically found in the breast. It is expected that total hemoglobin and water both increase in the fibroglandular tissue compared to the adipose tissue because of the increase in vasculature in the fibroglandular tissue.

A 33 yr old patient undergoing neo-adjuvant chemotherapy was scanned with the system 1 day after the second cycle of chemotherapy and 4 months before surgery. This patient had a 3cm invasive ductal carcinoma with 3 satellite lesions as identified by DCE-MR shown in Figure 5(a). Because this patient responded to chemotherapy, the recovered contrasts between the tumors and the fibroglandular tissue in the optical imaging plane were reduced compared to earlier in the treatment cycle, but were still evident at this stage. Optical and MR results from a later date (not shown) show very little contrast compared to the fibroglandular tissue. Recovered chromophore values are shown in Figure 5(b).

The values of total hemoglobin in the 2 tumor masses in the imaging plane were about 20 μM in the main lesion and about 19 μM in the satellite lesion in the plane of the optical fibers. These values are elevated compared to the fibroglandular tissue at 17 μM, and the adipose layer at 16 μM. This trend is expected in breast cancer because of the increased vasculature that is inherent to tumors, although the contrast in this imaging session is lower, most likely due to the response to chemotherapy treatment. The decreases in oxygen saturation from 75% in the fibroglandular tissue to 52% in the tumor masses are also expected because of the increase in

metabolic activity related to growth. In previous work, water has been shown to be elevated in tumor tissue, and the main lesion is slightly higher at 52% compared to 51% and 48% in the surrounding tissue. Interestingly, the satellite lesion is at the same water content as the fibroglandular, at 49%, perhaps indicating less inflammation than the main lesion. However, this result should be interpreted with less certainty because of the limitations in water recovery demonstrated in phantom imaging. Contrast is found in scattering amplitude in both lesions compared to the surrounding tissue, but not in scattering power. Scattering has been shown to correlate to microvascular density, and differences in microvascular density are expected in tumor tissue. These results were also compared to imaging results from a standalone optical tomography system (not shown), and quantification appears to be quite similar, although the spatial resolution of the standalone system is poorer because of the lack of MR guidance. Further investigations are underway to determine the benefits of using MR-NIRS for monitoring neoadjuvant chemotherapy.

Figure 6 shows examples of 3D interactive images of total hemoglobin, oxygen saturation, water, and scattering properties overlaid on the MR image for this subject. A closer inspection of the effect of scaling the transparency to the Jacobian can be seen in Figure 7. These datasets may be viewed interactively with Volview software, for further investigation.

4. Discussion

Diffuse optical tomography is inherently a 3D problem, and 3D models describe light propagation with more accuracy than 2D models. Additionally, radiologists and clinicians are accustomed to assessing lesions in 3 dimensions. However, non image-guided 3D-DOT is limited in its accuracy due to the ill-posed nature of the inversion problem and the fact that the problem is highly under-determined. Reducing the imaging problem to a NIR spectroscopy problem makes the solution more tractable and improves quantification. The MR-guided regionization process demonstrated here provides a huge reduction in memory usage and allows the overlay of optical data onto the MR scan without affecting the image resolution.

This paper has shown several examples of 3D image guided NIRS *in vivo*, with a goal of identifying the optimal way to visualize the data using tools which conform to existing radiological conventions. Phantom studies were completed to validate the contrast recovery, and show reasonable recovery of total hemoglobin in the inclusion. The recovered values for the subjects are within the physiologically expected range. These are the first published 3D MR guided optical images of healthy tissue and breast cancer, and the results in the malignancy show the expected increase in total hemoglobin and decrease in oxygen saturation.

An important exception to the expected values is the inaccuracy in the recovery of water concentration. This limitation is well known [35,36,37], and arises from the exclusion of longer wavelength diodes above 900nm which would better quantify the water spectrum. However, the photomultiplier tubes necessary for this application which need fast temporal response and high gain are not uniformly sensitive from 650nm – 950nm. This limitation yeilds crosstalk between water and oxyhemoglobin. Two approaches are currently underway to address this issue. One involves the use of spectrometers which are sensitive to these longer wavelengths and detect CW light. Coupling these detectors to PMTs would yield valuable quantification of water and lipids. The other approach is to use the MRs ability to separate water and fat. Assuming that the MR and optical are sensitive to the same water and fat, MR water quantification could be coupled to optical methods to further improve the accuracy of physiological parameters [38]. Previous studies [39] prove that this is true in oil/water phantoms.

5. Conclusions

This paper has presented the methodology of 3D segmentation, meshing, spectral fitting, and 3D visualization which enable optical imaging to become a viable, practical tool in the clinic, and was validated with phantoms and healthy and abnormal subjects. The main goal of MRNIRS is to help radiologists characterize suspicious lesions which have been located *a priori* with DCE-MRI. The steps transforming these MRI images into computational space have been presented and evaluated, with a key addition being a method of displaying the confidence in the optical recovery by scaling the transparency to the Jacobian matrix values in the 3D image. This visualization overlay conforms the optical contrasts to a fused MR dataset to appropriately display the tissue contrasts.

Acknowledgements

The authors gratefully thank the contributing radiologists Dr. Steven P. Poplack and Dr. Roberta M. diFlorio-Alexander, and the MRI technicians, Jorge A. Forero and Michael A. Pearl for their time and expertise. This work was funded by the Department of Defense Breast Cancer pre-doctoral fellowship (BC073418) and the National Cancer Institute (P01CA80139).

References and links

1. Bone B, Pentek Z, Perbeck L, Veress B. Diagnostic accuracy of mammography and contrast-enhanced mr imaging in 238 histologically verified breast lesions. Acta. Radiol 1997;38:489–496. [PubMed: 9240665]
2. Bluemke D, Gatsonis C, Chen M, DeAngelis G, DeBruhl N, Harms S, Heywang-Kobrunner S, Hylton N, Kuhl C, Lehman C, Pisano E, Causer P, Schnitt S, Smazal S, Stelling C, Weatherall P, Schnall M. Magnetic resonance imaging of the breast prior to biopsy. J. Am. Med. Assoc 2004;292:2735–2742.
3. Orel S, Schnall M. Mr imaging of the breast for detection, diagnosis, and staging of breast cancer. Radiology 2001;220:13–30. [PubMed: 11425968]
4. Hathaway P, Mankoff D, Maravilla K, Austin-Seymour M, Ellis G, Gralow J, Cortese A, Hayes C, Mode R. Value of combined fdg pet and mr imaging in the evaluation of suspected recurrent local-regional creast cancer: Preliminary experience. Radiology 1999;210:807–814. [PubMed: 10207485]
5. Catana C, Procissi D, Wu Y, Judenhofer M, Qi J, Pichler B, Jacobs R, Cherry S. Simultaneous in vivo positron emission tomography and magnetic resonance imaging. Proc. Natl. Acad. Sci. USA 2008;105:3705–3710. [PubMed: 18319342]
6. Sinkus R, Siegmann K, Xydeas T, Tanter M, Claussen C, Fink M. MR elastography of breast lesions: understanding the solid/liquid duality can improve the specificity of contrast-enhanced MR mammography. Magn. Reson. Med 2007;58:1135–1144. [PubMed: 17969009]
7. Van Houten E, Doyley M, Kennedy F, Weaver J, Paulsen K. Initial in vivo experience with steady-state subzone-based mr elastography of the human breast. J. Magn. Reson. Im 2002;17:72–85.
8. Ntziachristos V, Yodh AG, Schnall M, Chance B. Concurrent mri and diffuse optical tomography of breast after indocyanine green enhancement. Proc. Natl. Acad. Sci. USA 2000;97:2767–72. [PubMed: 10706610]
9. Ntziachristos V, Yodh AG, Schnall MD, Chance B. Mri-guided diffuse optical spectroscopy of malignant and benign breast lesions. Neoplasia 2002;4:347–54. [PubMed: 12082551]
10. Brooksby B, Jiang S, Dehghani H, Pogue BW, Paulsen KD, Kogel C, Doyley M, Weaver JB, Poplack SP. Magnetic resonance-guided near-infrared tomography of the breast. Rev. Sci. Instrum 2004;75:5262–5270.
11. Brooksby B, Pogue BW, Jiang S, Dehghani H, Srinivasan S, Kogel C, Tosteson T, Weaver JB, Poplack SP, Paulsen KD. Imaging breast adipose and fibroglandular tissue molecular signatures using hybrid mri-guided near-infrared spectral tomography. Proc. Natl. Acad. Sci. USA 2006;103:8828–8833. [PubMed: 16731633]
12. Townsend D, Cherry S. Combining anatomy and function: the path to true image fusion. Eur. Radiol 2001;11:1968–1974. [PubMed: 11702130]

13. Srinivasan S, Pogue BW, Brooksby B, Jiang S, Dehghani H, Kogel C, Wells WA, Poplack S, Paulsen KD. Near-infrared characterization of breast tumors in-vivo using spectrally-constrained reconstruction. Technol. Cancer Res. Treat 2005;4:513–526. [PubMed: 16173822]
14. Pogue BW, Poplack SP, McBride TO, Wells WA, S. OK, Osterberg UL, Paulsen KD. Quantitative hemoglobin tomography with diffuse near-infrared spectroscopy: Pilot results in the breast. Radiology 2001;218:261–266. [PubMed: 11152812]
15. Cerrusi A, Shah N, Hsiang D, Durkin A, Butler J, Tromberg B. In vivo absorption, scattering, and physiologic properties of 58 malignant breast tumors determined by broadband diffuse optical spectroscopy. J. Biomed. Opt 2006;11:044005. [PubMed: 16965162]
16. Fantini S, Walker SA, Franceschini MA, Kaschke M, Schlag PM, Moesta KT. Assessment of the size, position, and optical properties of breast tumors in vivo by noninvasive optical methods. Appl. Opt 1998;37:1982–1989. [PubMed: 18273118]
17. Grosenick D, Moesta K, Wabnitz H, Mucke J, Stroszczynski C, Macdonald R, Schlag P, Rinneberg H. Time-domain optical mammography: Initial clinical results on detection and characterization of breast tumors. Appl. Opt 2003;42:3170–3186. [PubMed: 12790468]
18. Chance B, Nioka S, Zhang J, Conant E, Hwang E, Briest S, Orel S, Schnall M, Czerniecki B. Breast cancer detection based on incremental biochemical and physiological properties of breast cancers: A six-year, two-site study. Acad. Radiol 2005;12:925–933. [PubMed: 16023383]
19. Poplack S, Tosteson T, Wells W, Pogue B, Meaney P, Hartov A, Kogel C, Soho S, Gibson J, Paulsen K. Electromagnetic breast imaging: Results of a pilot study in women with abnormal mammograms. Radiology 2007;243:350–359. [PubMed: 17400760]
20. Brooksby B, Jiang S, Dehghani H, Pogue BW, Paulsen KD, Weaver JB, Kogel C, Poplack SP. Combining near infrared tomography and magnetic resonance imaging to study in vivo breast tissue: implementation of a laplacian-type regularization to incorporate mr structure. J. Biomed. Opt 2005;10:050504−1−10.
21. Intes X, Maloux C, Guven M, Yazici T, Chance B. Diffuse optical tomography with physiological and spatial a priori constraints. Phys. Med. Biol 2004;49:N155–N163. [PubMed: 15272687]
22. Li A, Miller EL, Kilmer ME, Brukilaccio TJ, Chaves T, Stott J, Zhang Q, Wu T, Choriton M, Moore RH, Kopans DB, Boas DA. Tomographic optical breast imaging guided by three-dimensional mammography. Appl. Opt 2003;42:5181–5190. [PubMed: 12962399]
23. Yalavarthy P, Pogue B, Dehghani H, Carpenter C, Jiang S, Paulsen K. Structural information within regularization matrices improves near infrared diffuse optical tomography. Opt. Express 2007;15:8043–8058.
24. Carpenter C, Pogue B, Jiang S, Dehghani H, Wang X, Paulsen K, Wells W, Forero J, Kogel C, Weaver J, Poplack S, Kaufman P. Image-guided spectroscopy provides molecular specific information in vivo: Mri-guided spectroscopy of breast cancer hemoglobin, water, and scatterer size. Opt. Lett 2007;32:933–935. [PubMed: 17375158]
25. Dehghani H, Pogue BW, Jiang S, Brooksby BA, Paulsen KD. Three-dimensional optical tomography: resolution in small-object imaging. Appl. Opt 2003;42:3117–3128. [PubMed: 12790463]
26. McBride TO, Pogue BW, Gerety E, Poplack S, Osterberg UL, Paulsen KD. Spectroscopic diffuse optical tomography for quantitatively assessing hemoglobin concentration and oxygenation in tissue. Appl. Opt 1999;38:5480–90. [PubMed: 18324057]
27. Arridge SR, Schweiger M. Photon-measurement density functions. part 2: Finite-element-method calculations. Appl. Opt 1995;34:8026–8037.
28. Arridge SR, M. S, Delpy DT. Iterative reconstruction of near infrared absorption images. Proc. SPIE 1992;1767:372–383.
29. Corlu A, Choe R, Durduran T, Lee K, Schweiger M, Arridge SR, Hillman EM, Yodh AG. Diffuse optical tomography with spectral constraints and wavelength optimization. Appl. Opt 2005;44:2082–2093. [PubMed: 15835357]
30. Srinivasan S, Pogue BW, Jiang S, Dehghani H, Paulsen KD. Spectrally constrained chromophore and scattering nir tomography improves quantification and robustness of reconstruction. Appl. Opt 2004;44:1858–1869. [PubMed: 15813523]

31. McBride TO, Pogue BW, Jiang S, Osterberg UL, Paulsen KD. Development and calibration of a parallel modulated near-infrared tomography system for hemoglobin imaging in vivo. Rev. Sci. Instrum 2001;72:1817–1824.
32. Yalavarthy P, Pogue B, Dehghani H, Paulsen K. Weight-matrix structured regularization provides optical generalized least-squares estimate in diffuse optical tomography. Med. Phys 2007;34:2085. [PubMed: 17654912]
33. Schweiger M, Nissila I, Boas D, Arridge S. Image reconstruction in the presence of coupling errors. Appl. Opt 2007;46:2743–2756. [PubMed: 17446924]
34. Zhang J, Sullivan J, Yu H, Wu Z. Image-guided multimodality registration and visualization for breast cancer detection. Proc. SPIE 2005;5744:123–133.
35. Fantini S, Francheschini MA, Cerussi A, Maier JS, Walker SA, Barbieri B, Chance B, Gratton E. The effect of water in the quantitation of hemoglobin concentration in a tissue-like phantom by near-infrared spectroscopy. Biophys. J 1996;70:WP343–WP343.Part 2
36. McBride TO, Pogue BW, Jiang S, Osterberg UL, Paulsen KD, Poplack SP. Multi-spectral near-infrared tomography: a case study in compensating for water and lipid content in hemoglobin imaging of the breast. J. Biomed. Opt 2001;7:72–79. [PubMed: 11818014]
37. Cerussi AE, Jakubowski D, Shah N, Bevilacqua F, Lanning R, Berger AJ, Hsiang D, Butler J, Holcombe RF, Tromberg BJ. Spectroscopy enhances the information content of optical mammography. J. Biomed. Opt 2002;7:60–71. [PubMed: 11818013]
38. Li A, Boverman G, Zhang Y, Brooks D, Miller E, Kilmer M, Zhang Q, Hillman E, Boas D. Optical linear inverse solution with multiple priors in diffuse optical tomography. Appl. Opt 2005;44:1948–1956. [PubMed: 15813531]
39. Merritt S, Gulsen S, Chiou G, Chu Y, Deng C, Cerussi A, Durkin A, Tromberg B, Nalcioglu O. Comparison of water and lipid content measurements using diffuse optical spectroscopy and mri in emulsion phantoms. Technol. Cancer Res. Treat 2003;2:563–569. [PubMed: 14640767]

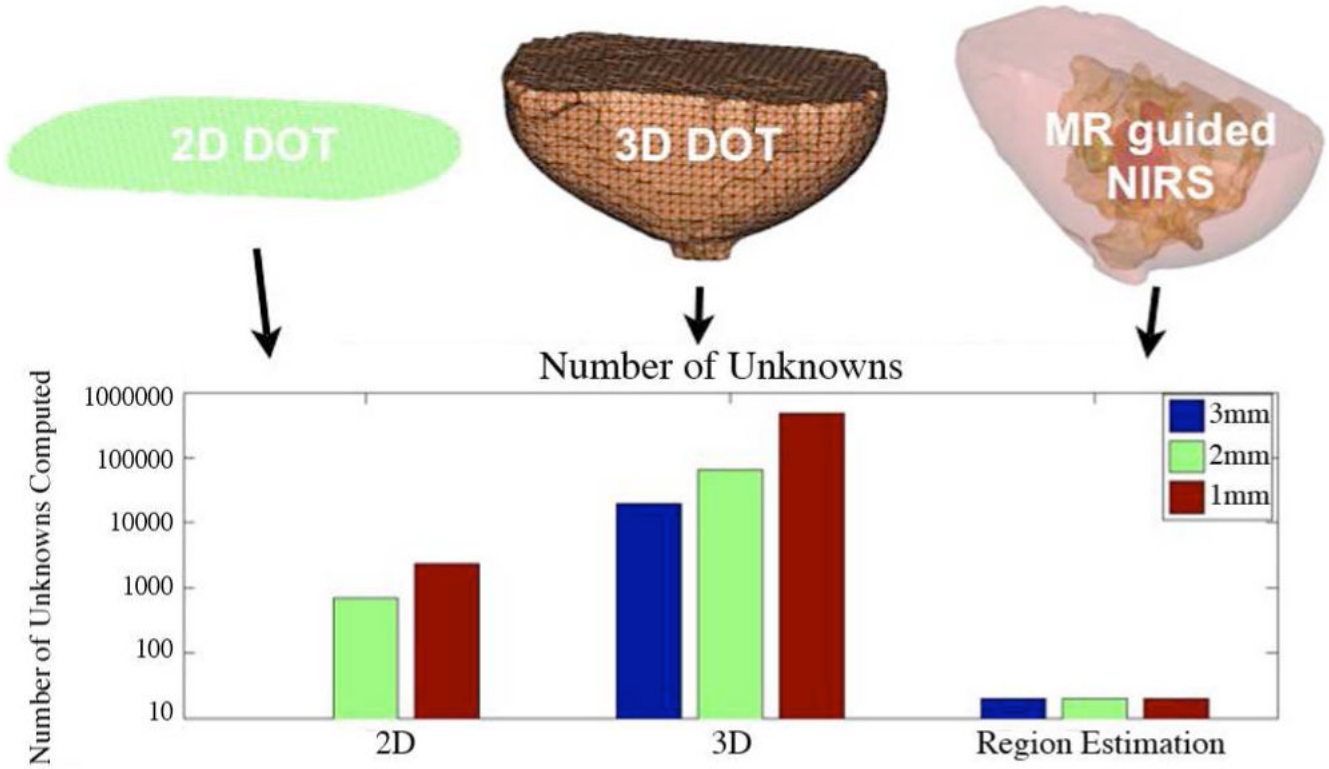

Fig. 1.
Comparison of the number of chromophores to be computed for 2D DOT, 3D DOT, and MR guided DOT.

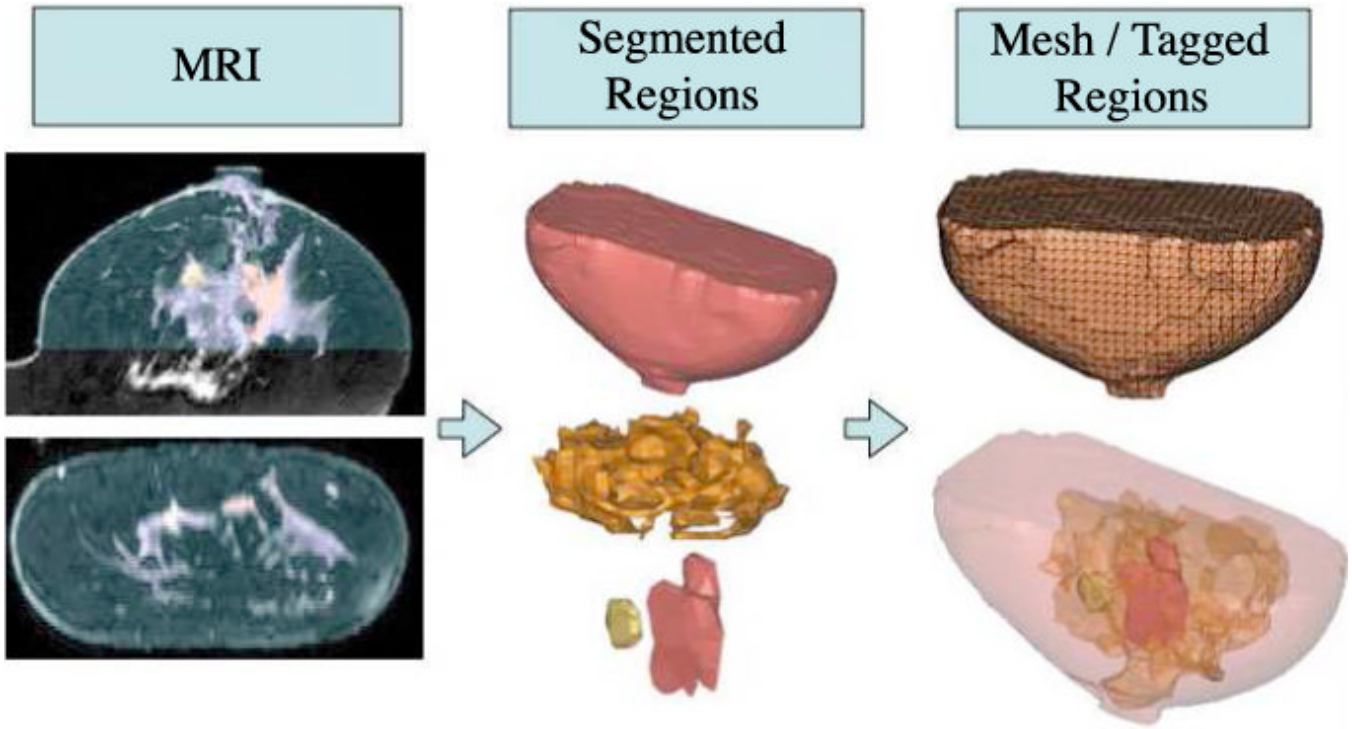

Fig. 2.
Transforming MRI images for computational use requires 1) Segmentation of tissue types into adipose, fibroglandular, and suspicious lesions, 2) Creating a finite element mesh of the volume from surface rendering, and 3) Tagging the mesh with tissue regions.

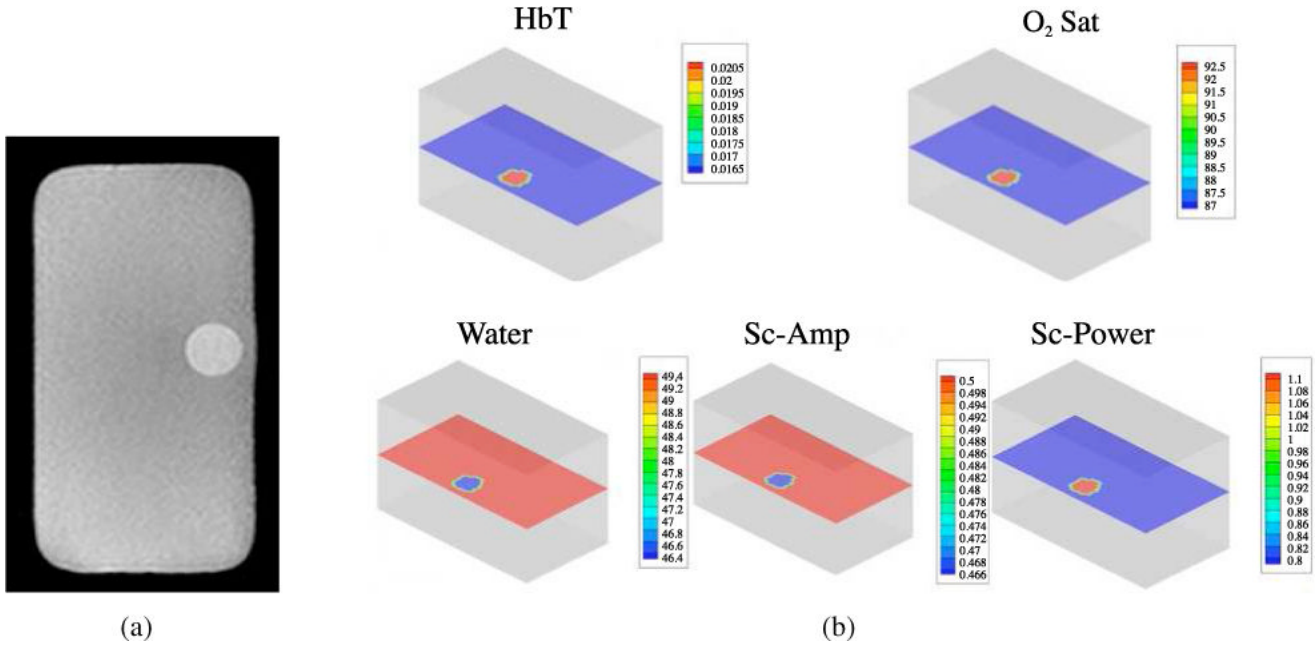

Fig. 3.

3D gelatin phantom results. (a) MR image of the gelatin phantom. (b) Total hemoglobin (in mM), Oxygen Saturation (in %), Water (in %), Scatter-Amplitude, and Scatter Power.

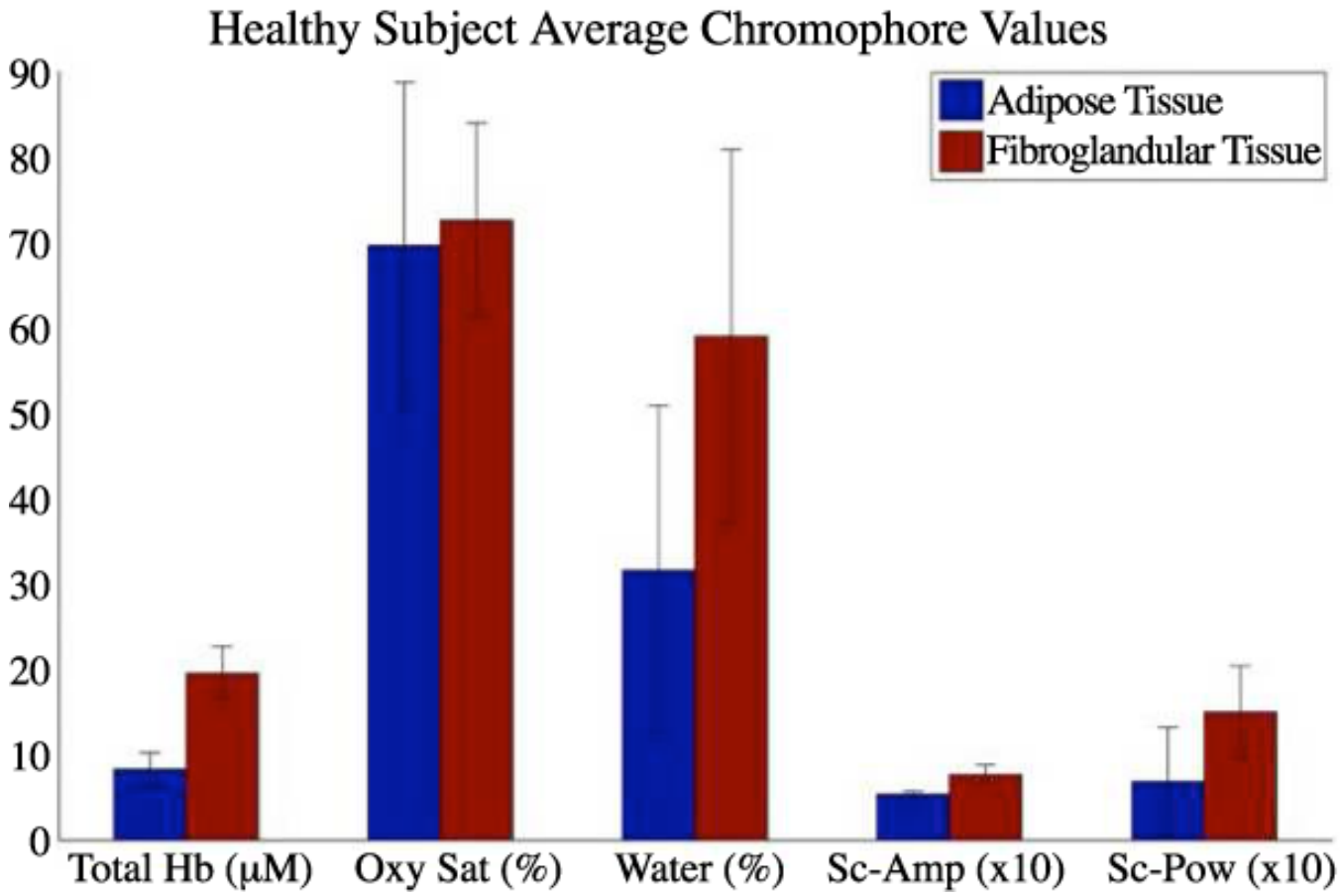

Fig. 4.
Mean and standard devation chromophore values for 3D recovered optical contrasts for 3 healthy subjects.

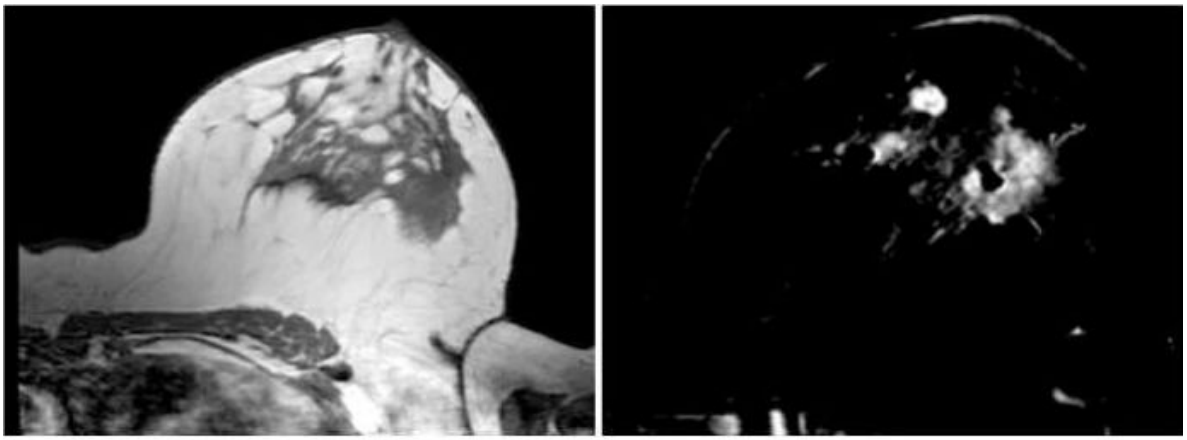

(a)

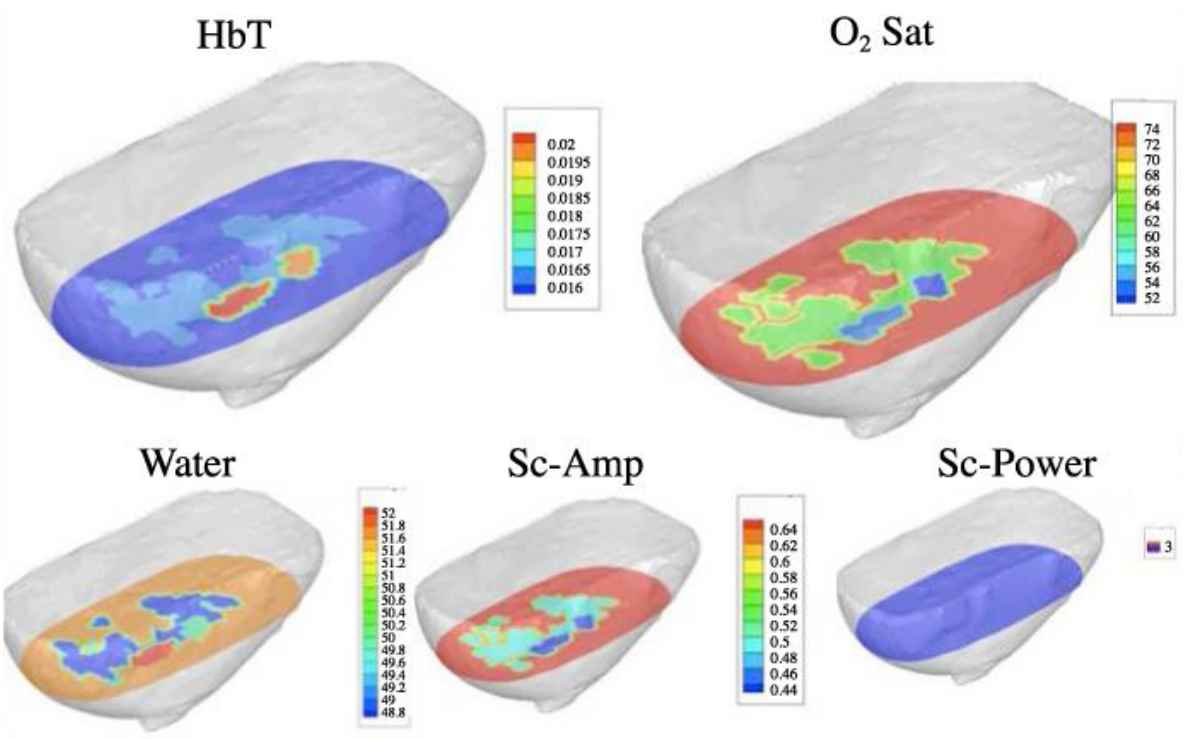

(b)

Fig. 5.

3D Reconstructed results of multi-focal IDC of the left breast. (a) Images of a malignant tumor with three satellite lesions (2 in plane):T1-W Spin Echo MRI image and DCE-MR subtraction image. (b) Images of a malignant tumor with three satellite lesions (2 in plane) Total hemoglobin, Oxygen Saturation, Water, Scatter Amplitude, and Scatter Power.

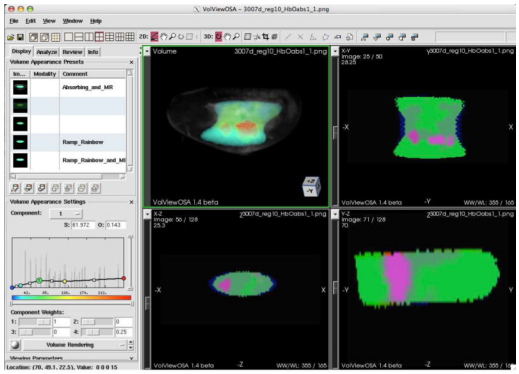

(a)

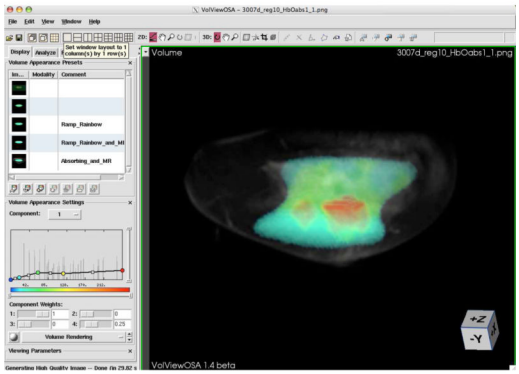

(b)

Fig. 6.

Optical and MR overlays of subject from Figure 5. (a) Composite image (View 1) of Optical absorbing images. (b) Total Hemoglobin (View 2), Oxygen Saturation (View 3), Water (View 4), Scatter Amplitude (View 5), and Scatter Power (View 6) images.

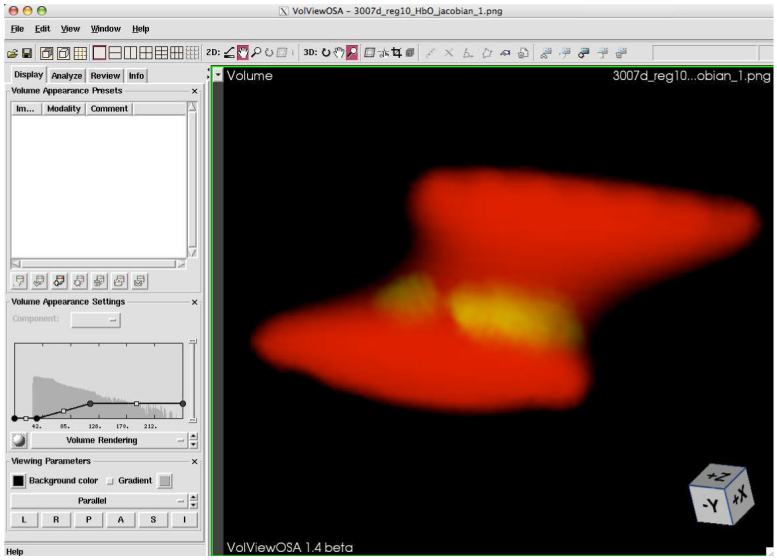

Fig. 7.
Effect of scaling the transparency of the recovered properties to the Jacobian. Interactive volume (View 7).